



NASA Technical Memorandum 4434

**Experimental Effects of Wing
Location on Wing-Body
Pressures at Supersonic Speeds**

Jerry M. Allen and Carolyn B. Watson

APRIL 1993



NASA Technical Memorandum 4434

Experimental Effects of Wing
Location on Wing-Body
Pressures at Supersonic Speeds

Jerry M. Allen and Carolyn B. Watson
Langley Research Center
Hampton, Virginia

NASA Technical Memorandum 4434

Abstract

An experimental study has been performed at supersonic speeds to measure wing and body spanwise pressure distributions on an axisymmetric-body delta wing model on which the wing vertical location on the body was systematically varied from low- to high-mounted positions. In addition, for two of these positions both horizontal and radial wing angular orientations relative to the body were tested, and roll angle effects were investigated for one of the positions. Seven different wing-body configurations and a body-alone configuration were studied. The test was conducted at Mach numbers from 1.70 to 2.86 at angles of attack from about -4° to 24° . Pressure orifices were located at three longitudinal stations on each wing-body model, and at each station the orifices were located completely around the body, along the lower surface of the right wing (looking upstream), and along the upper surface of the left wing. All pressure coefficient data are tabulated, and selected samples are shown graphically to illustrate the effects of the test variables. The effects of angle of attack, roll angle, Mach number, longitudinal station, wing vertical location, wing angular orientation, and wing-body juncture are analyzed. The vertical location of the wing on the body had a very strong effect on the body pressures. For a given angle of attack at a roll angle of 0° , the pressures were virtually constant in the spanwise direction across the windward surfaces of the wing-body combination. Pressure-relieving, channeling, and vortex effects were noted in the data.

Introduction

The airframe of tactical missiles has traditionally been composed of an axisymmetric body and one or more sets of fins mounted radially on the body; that is, the plane of the fins passes through the body axis of symmetry. However, advanced carriage and fin-folding considerations can result in missile designs that have planar fins mounted either high or low on the body. In either case, these fins do not extend through the body symmetry axis and thus are termed "off-axis" fins.

Little experimental data exist on this off-axis-fin class of configurations, although a recent computational study (ref. 1) was performed using an Euler code to estimate wing-body interference effects. The primary purpose of the present experimental study was to provide a systematic set of pressure data for a generic off-axis configuration. To facilitate comparisons with other developing computational methods, the surface pressure orifices on the model were located so that a set of data could be generated completely around the wing-body configuration at constant longitudinal stations. The model was designed to have a planform similar to the wing-body portion of the force-and-moment model of reference 2 so

that pressure and loads data would be available for comparison purposes.

Symbols

The capitalized expression in parentheses next to the symbol is the computer printout equivalent of that symbol that is used in the aerodynamic data presented in tables 3–10.

C_p	(CP)	pressure coefficient, $(p - p_\infty)/q_\infty$
M_∞		free-stream Mach number
p		static pressure on body or wing surface, psi
p_∞		free-stream static pressure, psi
q_∞		free-stream dynamic pressure, psi
S	(S)	distance from body centerline to wing trailing-edge tip, 4.82 in.
y	(Y)	spanwise wing coordinate (measured from body center- line), in.

α	(ALPHA)	model angle of attack, deg
θ	(THETA)	circumferential body coordinate (measured clockwise from windward meridian at roll angle of 0°, looking upstream), deg
ϕ	(PHI)	model roll angle (measured clockwise, looking upstream, from windward meridian), deg

Apparatus and Test

Wind Tunnel

The test was conducted in the low Mach number test section of the Langley Unitary Plan Wind Tunnel. This tunnel is a variable-pressure continuous-flow facility with two test sections ranging in Mach number from 1.47 to 4.63. The Mach number is controlled by asymmetric sliding blocks, and the low-speed test section has a Mach number variation from 1.47 to 2.90. The test section is formed by the downstream section of the nozzle and is approximately 4 ft wide by 4 ft high by 7 ft long. A more detailed description of this wind tunnel can be found in reference 3.

Model

The model is composed of an axisymmetric body with a three-caliber tangent-ogive nose and delta wings with a leading-edge sweep of 77°. Interchangeable wings were designed to be mounted at various vertical and angular positions on the body at the same streamwise location. This arrangement resulted in seven different wing-body configurations in addition to a body-alone (body without wings) configuration. The model with planar wings (zero dihedral) located along the body axis of symmetry was considered the baseline configuration. Pressure orifices were located at three longitudinal stations on each configuration, and figure 1 shows sketches of the baseline configuration and the longitudinal location of the pressure orifices. The eight test configurations are identified in figure 2, and photographs of all eight sting-mounted models are shown in figure 3.

A planform sketch of the baseline model is presented in figure 4 to show the important dimensions. As seen in this figure, the model semispan measured from the body centerline was 4.82 in., which was held constant for all the winged configurations. Thus, the exposed wing area increased as the wing was moved to high or low locations from the baseline configuration. Also shown in figure 4 are the three longitudinal

stations at which pressure orifices were located on the wings and body. These locations were chosen to be at about 50, 75, and 95 percent of the theoretical wing root chord when extended to the body centerline, and they are identified as stations 1, 2, and 3, respectively.

At each station the pressure orifices were located completely around the body, along the upper surface of the left wing (looking upstream), and along the lower surface of the right wing. Body pressure orifices were located in 15° increments around the body, which resulted in a maximum of 24 body orifices at each station for the body-alone configuration. The winged configurations had up to five fewer body orifices because of the intersection of the wings with the body. Figure 5, which is a cross-sectional sketch showing the location of the body orifices, indicates the orifices that were eliminated because of the various wing locations. This sketch is applicable to all three longitudinal stations.

The wing pressure orifices were located as shown in figure 6, which is representative of either the upper surface of the left wing or the lower surface of the right wing. As many as 10 orifices were located on each wing surface at each station. These orifices were positioned to lie along constant rays originating from the theoretical wing apex. Table 1 lists the locations of these orifices and the rays on which they are found. Note that the spanwise distance coordinate y is measured along the wing surface and, thus, does not lie in a horizontal plane for the radially mounted wings. Up to five inboard wing orifices were located inside the body for some of the wing positions, thereby reducing the number of usable wing orifices for those configurations.

The body-alone configuration contained a total of 72 pressure orifices, whereas the wing-body configurations contained between 106 and 114 usable orifices. All pressure orifices were 0.026 in. in diameter and were mounted flush with and normal to the body or wing surface.

The pressure orifices were located on a flat wing surface. A sharp 10° bevel perpendicular to the edge was provided on both the leading and trailing edges of the opposite surface of that wing to provide a structural thickness and to accommodate the internal pressure tubing. As stated previously, the right and left wings of each configuration were instrumented on opposite surfaces; therefore, the flat surface of each wing was located on opposite sides. For all configurations in this study, the pressure orifices were located on the lower surface of the right wing (looking upstream) and on the upper surface of the

left wing. Thus, the lower surface of the right wing and the upper surface of the left wing were always flat. Because of this difference between the right and left wing surfaces, none of the configurations, except for the body alone, had true symmetry about the vertical plane. All wings had a maximum thickness of 0.188 in.

Instrumentation

The model pressures were measured by three 48-channel, electronically scanned pressure (ESP) modules located inside the body. The operational range of these modules was ± 5 psid over a temperature range from 0°F to 175°F . The rated accuracy of the modules was ± 0.15 percent of the full-scale value. For the test conditions of this investigation, this accuracy corresponded to an agreement in pressure coefficient of about 0.004 to 0.008.

Flexible tubing was used to connect the pressure orifices to the ESP modules inside the body. Because of the limited space available inside the body to house the three ESP modules and the associated pressure tubing, a few tubes for some of the configurations became too constricted to allow an accurate pressure measurement when the model was assembled. The pressures measured from these orifices were eliminated from the results of this study.

The model angle of attack, which was measured using an accelerometer mounted inside the nose of the model, was corrected for wind tunnel flow angularity. Model roll angle was set using the tunnel roll mechanism.

To induce boundary-layer transition to turbulent flow, transition strips were applied to the model using the technique established in reference 4. This technique was also used in the force and moment test of reference 2. These transition strips consisted of No. 50 sand grains (0.0128 in.) sprinkled in acrylic plastic. The strips were 0.062 in. wide and were located 1.20 in. aft of the nose and 0.40 in. aft of the leading edges (measured streamwise) on both the upper and lower surfaces of the wings.

Tests

Tests on all configurations were conducted at Mach numbers of 1.70, 2.16, 2.40, and 2.86 at a Reynolds number of 2×10^6 per foot. The model angle of attack ranged from about -4° to 24° in increments of 4° . The effects of roll angle ϕ were studied on the baseline configuration only (configuration 1), and for this configuration the roll angle varied from -90° to 90° in 30° increments.

Presentation of Data

Table 2 shows the arrangement of the pressure coefficient data listed in tables 3–10. Body pressure data are tabulated as a function of angular location around the body (θ), whereas the wing pressure data are tabulated as a function of the nondimensional distance along the wing from the body centerline (y/S). Note that the y/S parameter is measured along the wing surface which does not lie in a horizontal plane for the radially mounted wings. Selected data from tables 3–10 have been plotted and are analyzed in the following sections of this paper to illustrate the effects of the test variables. More extensive plots of the pressure data along with selected vapor-screen photographs of the vortex patterns on the model can be found in reference 5.

Analysis of Selected Data

The primary test variables in this investigation are the model angle of attack and roll angle, the free-stream Mach number, and the wing vertical location and angular orientation on the body. The effects of longitudinal station and wing-body juncture can also be examined because data were obtained at three streamwise locations on both the wings and body.

The effects of the resulting seven variables are examined sequentially in this section. All pressure coefficient data have been plotted to the same scale to facilitate comparisons. Body pressure data are plotted as a function of angular location around the body (θ). For $\phi = 0^\circ$, the windward meridian on the body is located at $\theta = 0^\circ$ and 360° , whereas the leeward meridian is located at $\theta = 180^\circ$. Wing pressures are plotted as a function of the nondimensional spanwise distance y/S along the wing from the body centerline.

For all wing pressure plots at $\phi = 0^\circ$ discussed in the following sections of this paper, windward and leeward pressures are shown together as if they were measured on windward and leeward surfaces of the same wing, even though they were, in fact, measured on opposite wings. For these cases, the plots are presented in this manner to facilitate comparisons between windward and leeward pressures and to emphasize that a set of pressure data encompassing the wing-body combination can be generated from these data. Data for nonzero roll angles need to be presented in a different manner, as will be discussed later when examining roll angle effects.

Effect of Angle of Attack

The effect of angle of attack on body and wing pressures is examined in this section for the body

alone (configuration 8) and for the baseline wing-body model (configuration 1). Data obtained at some of the intermediate angles of attack are not included on the plots for clarity.

The effect of angle of attack on the body-alone pressures is shown in figure 7 for station 3 at $M_\infty = 1.70$. As would be expected, the pressures on the windward side of the body increase with angle of attack and decrease on the leeward side of the body. At the higher angles of attack, the windward pressures decrease rapidly around the body and reach a minimum at about $\theta = 75^\circ$, or at 285° on the opposite side of the body, before recovering and remaining almost constant over the leeward surface. These minimums are probably due to vortices separating from the body at these locations.

Pressures on the baseline configuration (configuration 1) are shown in figure 8, where the test conditions are the same as those in figure 7. Comparing the body pressures on configuration 1 (fig. 8(a)) with the body-alone pressures of figure 7 shows a very large angle-of-attack effect because of the presence of the wings. At similar angles of attack, the wings cause much higher pressures on the windward side of the body and much lower pressures on the leeward side. Also, the wings cause the windward pressures to be relatively constant compared with the body-alone pressures. Notice that a sharp increase in pressure develops on the body at the higher angles of attack near the leeward meridian for configuration 1. This trend was not seen in the body-alone data.

The pressures on the wing for configuration 1 are shown in figure 8(b). The windward surface pressures increase systematically with angle of attack and are nearly constant in the spanwise direction. On the leeward wing surface, pressure decreases with angle of attack except at 7.17° and 15.19° when an increase occurs on the inboard part of the wing as compared with the outboard part. This pattern is typical of a classic leading-edge vortex on delta wings that was discussed in reference 6.

Effect of Roll Angle

Figure 9 shows the effect of roll angle on the pressures on configuration 1 at station 3 for $M_\infty = 1.70$ and $\alpha \approx 20^\circ$. Note that the body angular coordinate θ is fixed to the body and thus rotates with roll angle ϕ relative to the free-stream cross flow direction. For this reason the body pressures in this figure have been plotted as a function of $\theta + \phi$ so that the data can be compared at the same location on the body relative to the free-stream cross flow direction. (See the sketch in fig. 9(a).)

Figure 9(a) shows that roll angle has a strong effect on the body pressures, but for clarity, only positive roll angles are shown. For the nonsymmetrical roll angles, the maximum body pressures occur near the wing on the windward side, and the minimum pressures occur near the leeward side of that same wing.

Figure 9(b) shows roll angle effects on the wing pressures. Because of the location of the wing pressure orifices, the nonzero roll angle data in this figure are no longer representative of windward and leeward pressures on the same wing. Rather, these data are from the windward side of the lower wing and from the leeward side of the upper wing. Because vertical flow symmetry no longer applies, these data can no longer be used at a given roll angle to generate a complete data plane around the configuration.

This data plane can still be extracted from the test data in this study, however, by combining the results from positive and negative roll angles. A sample of such a combination is shown in figure 9(c) in which data from positive and negative roll angles of 30° have been combined to give a data plane over the complete wing-body combination. These data are from configuration 1 at station 3 for $\alpha \approx 20^\circ$. Note that the body pressures have been included in this figure at their corresponding values of y/S to show how a complete wing-body data plane can be constructed.

Effect of Mach Number

The effect of Mach number is discussed with the aid of figure 10 which contains data from configuration 1 at station 3 for $\alpha \approx 20^\circ$ and $\phi = 0^\circ$. Figure 10(a) shows the effect of body pressures. Even though Mach number has very little effect on the windward side of the body, a large systematic increase in body pressure occurs on the leeward side. At all Mach numbers the pressures increase sharply near the leeward meridian, which in previous discussions was attributed to the presence of the wing.

Figure 10(b) shows a similar trend in the wing pressures; that is, they are almost constant on the windward surface and systematically increase with Mach number on the leeward surface. Notice that the effect of the wing leading-edge vortex decreases with Mach number, as seen by the increase in pressures near the leeward meridian at $y/S = 0.4$ and 0.5 .

Effect of Longitudinal Station

Figure 11 shows the pressures at the three longitudinal stations for configuration 1 at $M_\infty = 1.70$, $\alpha = 19.23^\circ$, and $\phi = 0^\circ$. Figure 11(a) shows that the

pressures on the windward side of the body are nearly constant between stations 2 and 3 but are significantly lower at station 1. On the leeward surface of the body as noted earlier, the increase in pressures near the leeward meridian is seen to continually increase down the length of the body.

Figure 11(b) shows that the pressures on both surfaces of the wing are nearly constant with longitudinal station. The leeward pressures show the progression of the wing leading-edge vortex as it moves downstream over the configuration.

Effect of Wing Vertical Location

Figure 12 shows the effect of the wing vertical location. In this figure the effects of moving the horizontal wing from low to high on the body are examined by comparing data from configurations 1–5 at $M_\infty = 1.70$, $\alpha \approx 20^\circ$, and $\phi = 0^\circ$.

Figure 12(a) shows that the wing vertical location on the body has a very large effect on the body pressures. The wing location essentially acts as a dividing line between the windward and leeward pressure levels for all wing locations. For example, all body pressures for the highest mounted wing (configuration 2) are at the level of the windward pressures, whereas all body pressures for the lowest mounted wing (configuration 5) appear as leeward pressures.

In contrast, figure 12(b) shows that the wing vertical location has a much smaller effect on the wing pressures. On the low-mounted configurations, the pressures on the windward surface are almost constant over the wing span, and some effects of the body can be seen on the inboard part of the windward surfaces for the high-mounted configurations. On the leeward surface of the wing, the largest effect of the wing vertical location is also seen on the inboard part of the wing.

Effect of Wing Angular Orientation

Configurations 6 and 7 are the only wing-body configurations in this study in which the wings are not located in a horizontal plane but extend radially from the body in high- and low-mounted positions. Configurations 3 and 5 have horizontal wings mounted at the same locations as those of configurations 6 and 7, respectively. Therefore, comparisons between the data from configurations 3 and 6 and configurations 5 and 7 show the effect of angular orientation of the wings. These comparisons are made in figures 13 and 14 for $M_\infty = 1.70$ at station 3 for $\alpha \approx 20^\circ$.

Figure 13 shows the effect of wing angular orientation for the high-mounted wings (configurations 3 and 6). The effect on the body (fig. 13(a)) is confined primarily to the windward side where the horizontal wings are seen to produce the higher pressures. Therefore, rotating the wings from the horizontal to the radial position for these high-mounted wings acts to relieve the pressures on the windward side of the body but has little effect on the leeward pressures. A similar relieving effect is seen on the windward surface of the wings (fig. 13(b)). The closer proximity of the leading-edge vortex to the wing surface for the horizontal wing results in significantly lower pressures on the leeward surface of that wing.

Figure 14 shows the effect of wing angular orientation for the low-mounted wings (configurations 4 and 7). In contrast to the high-mounted case, figure 14(a) shows a large effect on the body pressures on the leeward surface, with the horizontal wings creating the lower pressures. The pressures for both wing orientations are nearly constant on the windward body surface, with the radially mounted wing producing the higher pressures. In fact, for the same angle of attack, the channeling effect of the wings on configuration 7 produced the highest body pressures measured on any configuration in this study.

Figure 14(b) shows that the pressures on the windward surface of the wings of both configurations are almost constant in the spanwise direction, again with the radially mounted wing producing the higher pressures. The pressures on the outboard part of the leeward wing surface are similar for the two configurations, but they diverge on the inboard part because of the closer proximity of the leading-edge vortex to the radially mounted wing surface.

Effect of Wing-Body Juncture

All body pressures presented thus far, except for those illustrating roll angle effects in figure 9(c), have been plotted as a function of angular location on the body (θ), whereas the wing pressures have been plotted as a function of the spanwise dimension parameter (y/S). In order to compare wing and body pressures directly in the vicinity of the wing-body juncture, figure 15 was prepared in which the location of the body pressure data was transformed from the angular location (θ) to the corresponding value of the spanwise parameter (y/S). Data are presented in figure 15 for all wing-body configurations investigated in this study at $M_\infty = 1.70$, station 3, $\alpha \approx 20^\circ$, and $\phi = 0^\circ$.

Figure 15(a) presents data from the baseline model (configuration 1). The pressures over the

windward surface are seen to be virtually constant over the span of the entire wing-body combination. The pressures on the leeward side, however, are much higher on the body than on the wing except in the vicinity of the wing-body juncture where a smooth transition takes place.

The “looping” effect in the data from the other configurations, seen in figures 15(b)–15(g), is the result of the double values of the y/S parameter when the wing is not located on the body centerline. The pressures over the entire windward wing-body combination were virtually constant in the spanwise direction for all configurations except configuration 6 (fig. 15(b)) because of the pressure-relieving effect noted earlier for that configuration. Note that no leeward body pressures exist for the highest mounted configuration (fig. 15(b)) and, conversely, no windward body pressures exist for the lowest mounted configuration (fig. 15(e)).

Concluding Remarks

An experimental study has been performed at supersonic speeds to obtain spanwise pressure distributions on an axisymmetric-body delta wing configuration in which the wing vertical and angular locations on the body were systematically varied. Pressure coefficient data for the entire investigation are listed in tabular form. Selected samples from these data are presented graphically to illustrate the effects of angle of attack, roll angle, Mach number, longitudinal station, wing vertical location, wing angular orientation, and wing-body juncture.

The vertical location of the wing on the body was found to have a very strong effect on the body

pressures. For a given angle of attack at a roll angle of 0° , the pressures were virtually constant in the spanwise direction across the windward surfaces of the wing-body combination. Pressure-relieving, channeling, and vortex effects were noted in the data.

NASA Langley Research Center
Hampton, VA 23681-0001
February 23, 1993

References

1. Jenn, A. A.; and Nelson, H. F.: Wing Vertical Position Effects on Lift for Supersonic Delta Wing Missiles. *J. Spacecr. & Rockets*, vol. 26, no. 4, July–Aug. 1989, pp. 210–216.
2. Blair, A. B., Jr.: *Effect of Wing Location and Strakes on Stability and Control Characteristics of a Monoplanar Circular Missile With Low-Profile Tail Fins at Supersonic Speeds*. NASA TM-81878, 1980.
3. Jackson, Charlie M., Jr.; Corlett, William A.; and Monta, William J.: *Description and Calibration of the Langley Unitary Plan Wind Tunnel*. NASA TP-1905, 1981.
4. Stallings, Robert L., Jr.; and Lamb, Milton: *Effects of Roughness Size on the Position of Boundary-Layer Transition and on the Aerodynamic Characteristics of a 55° Swept Delta Wing at Supersonic Speeds*. NASA TP-1027, 1977.
5. Fulton, Patsy S.: *Wind Tunnel Pressure Study and Euler Code Validation of a Missile Configuration With 77° Swept Delta Wings at Supersonic Speeds*. NASA TM-101531, 1988.
6. Miller, David S.; and Wood, Richard M.: *Lee-Side Flow Over Delta Wings at Supersonic Speeds*. NASA TP-2430, 1985.

Table 1. Spanwise Locations of Wing Orifices

Station	y , in.	y/S	Ray
1	0.241	0.050	1
	.482	.100	2
	.723	.150	3
	.964	.200	4
	1.205	.250	5
	1.446	.300	6
	1.687	.350	7
	1.929	.400	8
	2.049	.425	9
	2.170	.450	10
2	0.361	0.075	1
	.722	.150	2
	1.083	.225	3
	1.444	.300	4
	1.806	.375	5
	2.167	.450	6
	2.528	.524	7
	2.889	.599	8
	3.070	.637	9
	3.250	.674	10
3	0.914	0.190	2
	1.321	.274	3
	1.829	.379	4
	2.281	.473	5
	2.743	.569	6
	3.200	.664	7
	3.657	.759	8
	3.886	.806	9
	4.114	.854	10

Table 2. Arrangement of Tables 3–10

(a) Configuration 1 (table 3)

Mach number	Part of table 3 for roll angle, ϕ , of—						
	0°	30°	60°	90°	-30°	-60°	-90°
1.70	(a)	(e)	(i)	(m)	(q)	(u)	(y)
2.16	(b)	(f)	(j)	(n)	(r)	(v)	(z)
2.40	(c)	(g)	(k)	(o)	(s)	(w)	(aa)
2.86	(d)	(h)	(l)	(p)	(t)	(x)	(bb)

(b) Configurations 2–8 (tables 4–10) with $\phi = 0^\circ$

Mach number	Part found in table—						
	4	5	6	7	8	9	10
1.70	(a)	(a)	(a)	(a)	(a)	(a)	(a)
2.16	(b)	(b)	(b)	(b)	(b)	(b)	(b)
2.40	(c)	(c)	(c)	(c)	(c)	(c)	(c)
2.86	(d)	(d)	(d)	(d)	(d)	(d)	(d)

(a) Bottom oblique view.

(b) Top oblique view.

Figure 1. Baseline model showing pressure orifice locations.

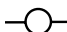
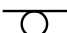






Configuration	Configuration description	Identification symbol
1	Horizontal wings mounted at body centerline (baseline configuration)	
2	Horizontal wings mounted on top of body	
3	Horizontal wings mounted midway between body centerline and top of body	
4	Configuration 3 rolled 180°	
5	Configuration 2 rolled 180°	
6	Radially mounted wings at same location as on configuration 3	
7	Configuration 6 rolled 180°	
8	Body alone (without wings)	

Figure 2. Description of test configurations shown in figures 7–15.

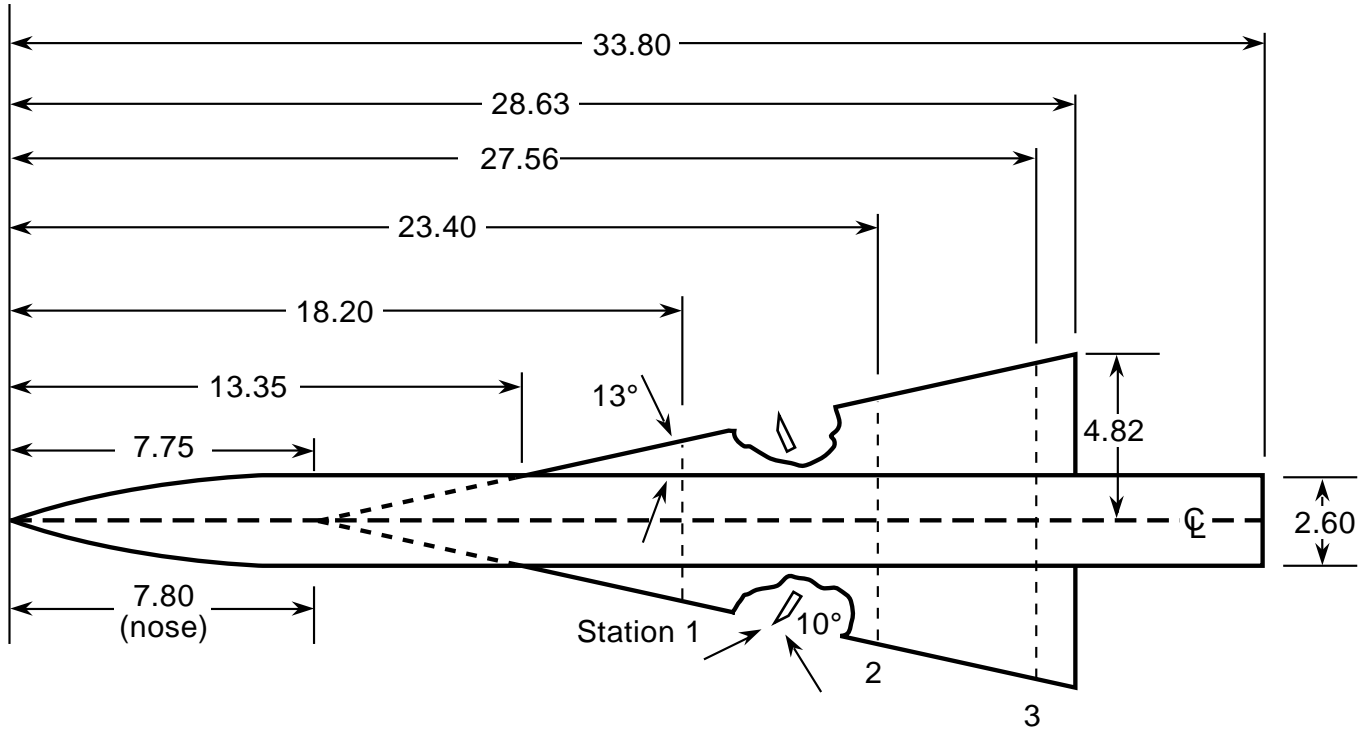


Figure 4. Dimensions of configuration 1. Linear dimensions are given in inches.

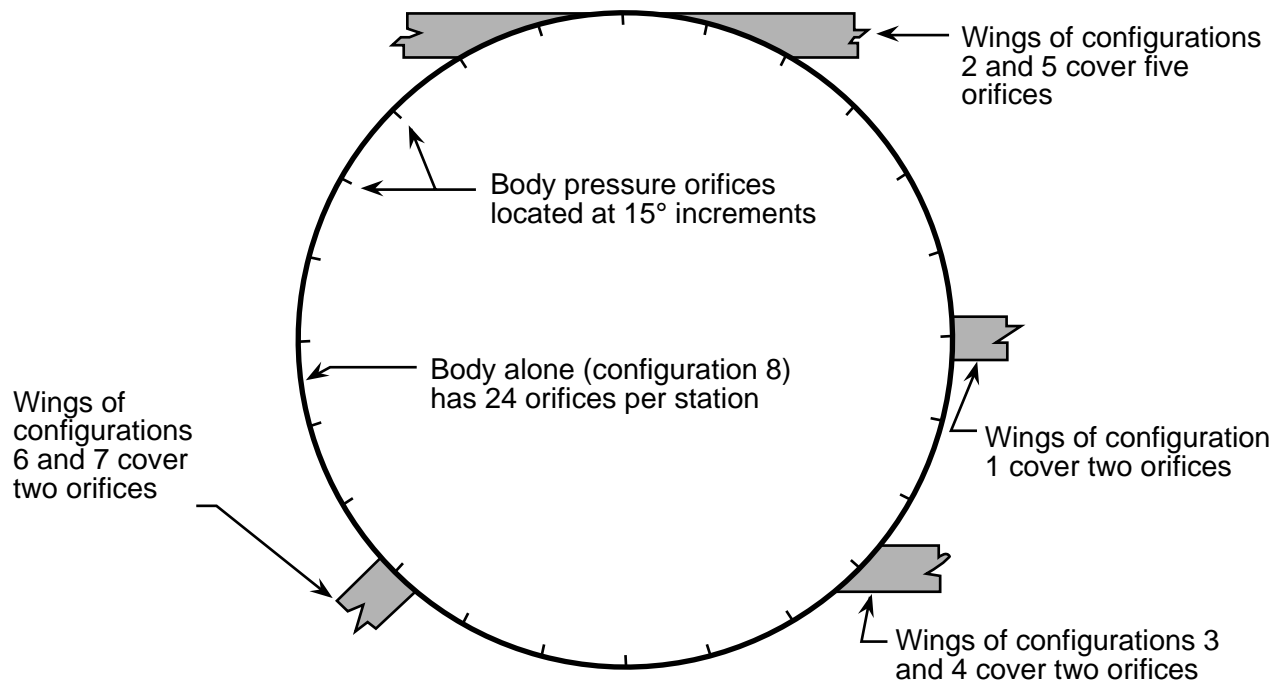


Figure 5. Locations of body pressure orifices.

Figure 6. Locations of wing pressure orifices.

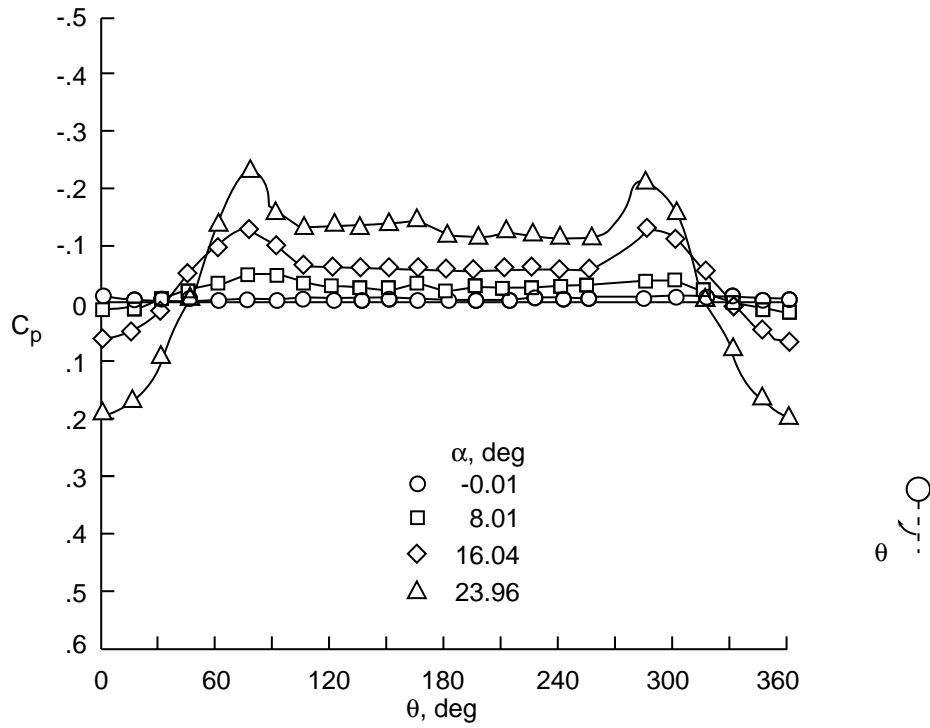
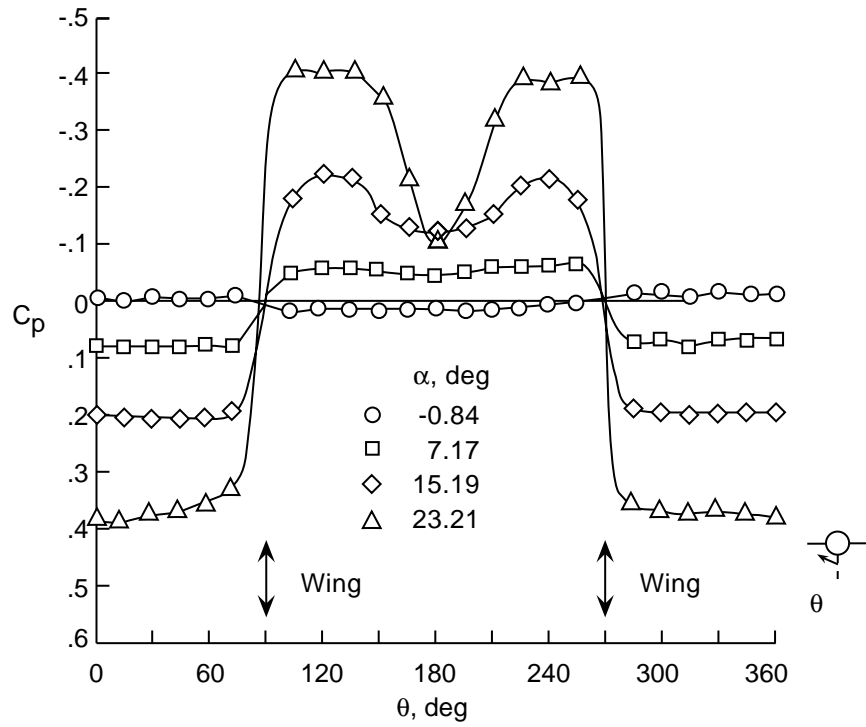
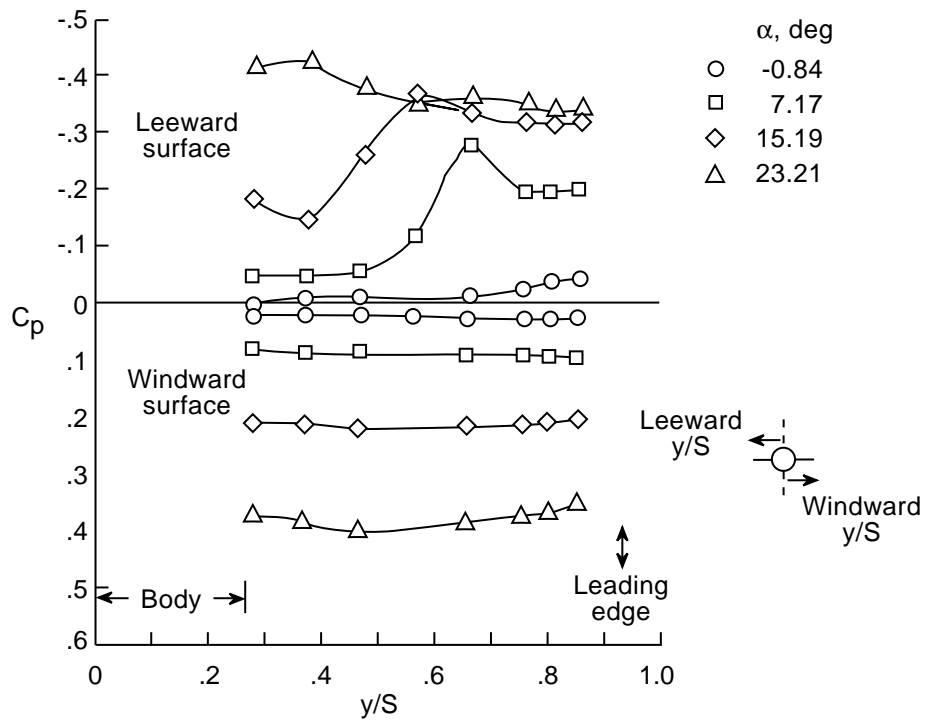


Figure 7. Pressure distributions around station 3 of configuration 8 (body alone) at $M_\infty = 1.70$ and $\phi = 0^\circ$.

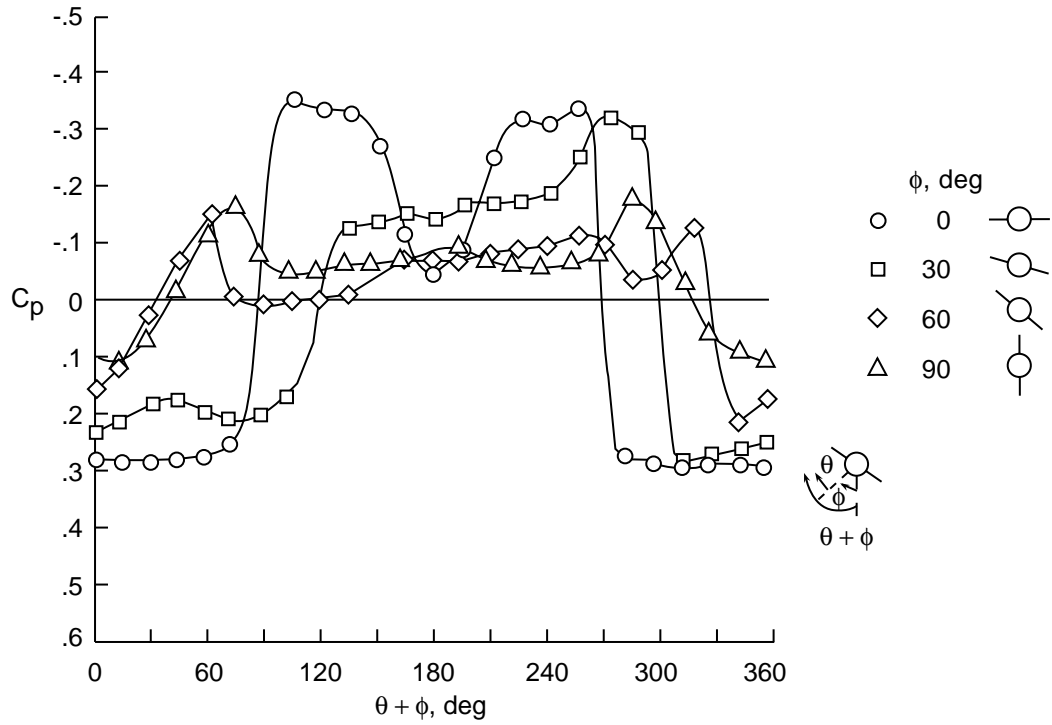


(a) Body.

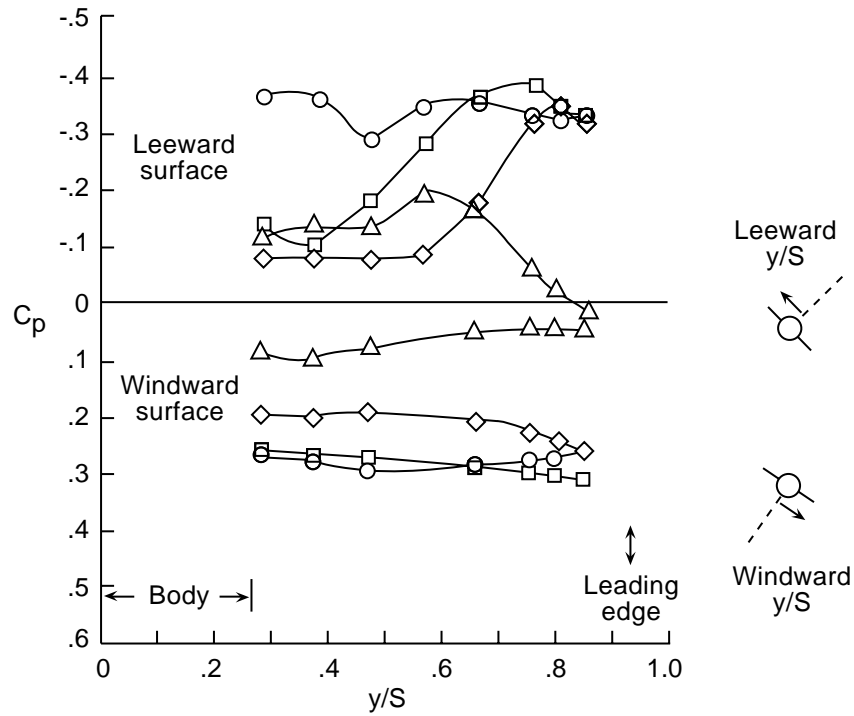


(b) Wing.

Figure 8. Effect of angle of attack on station 3 of configuration 1 at $M_\infty = 1.70$ and $\phi = 0^\circ$.

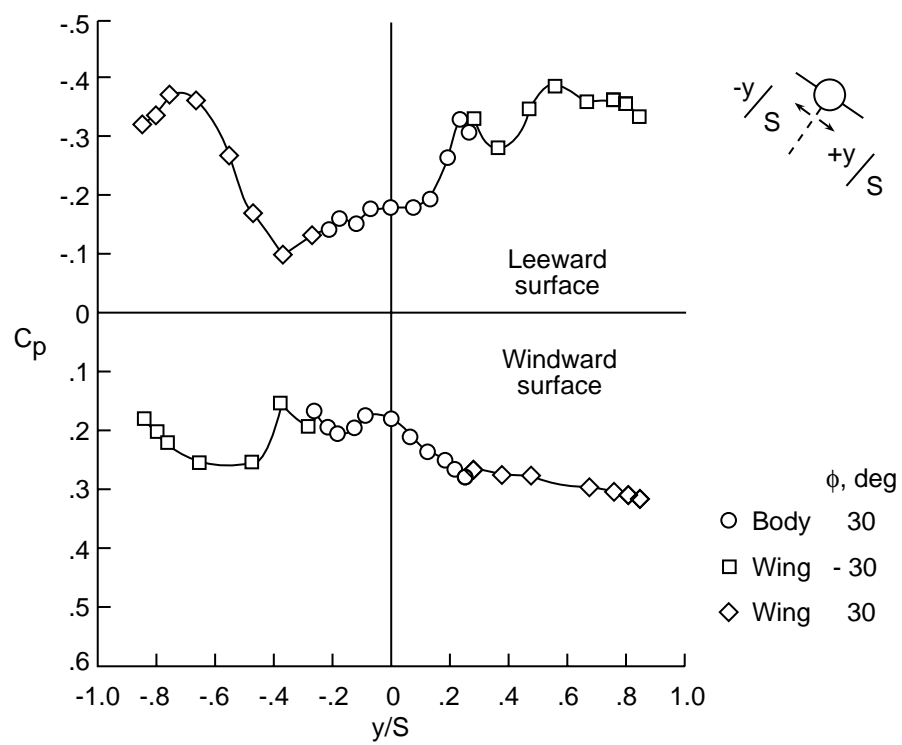


(a) Body.



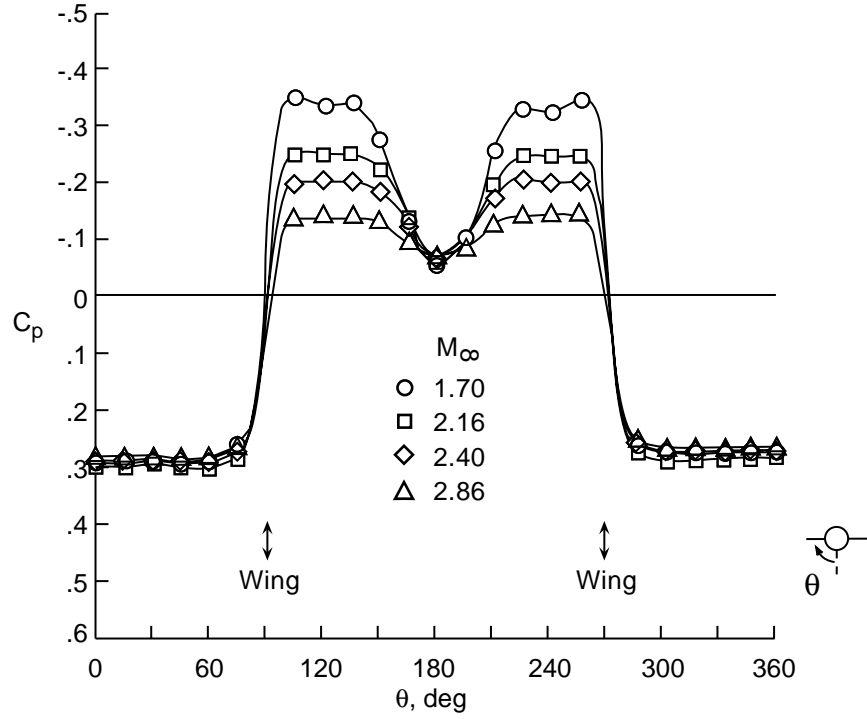
(b) Wing.

Figure 9. Effect of roll angle on station 3 of configuration 1 at $M_\infty = 1.70$ and $\alpha \approx 20^\circ$.

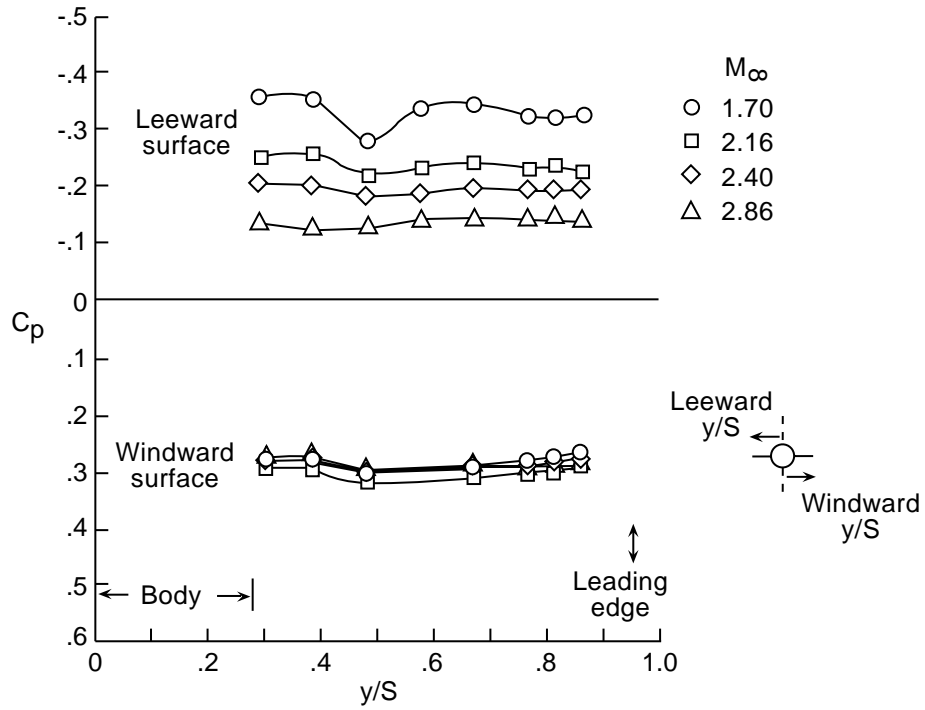


(c) Wing-body combination.

Figure 9. Concluded.

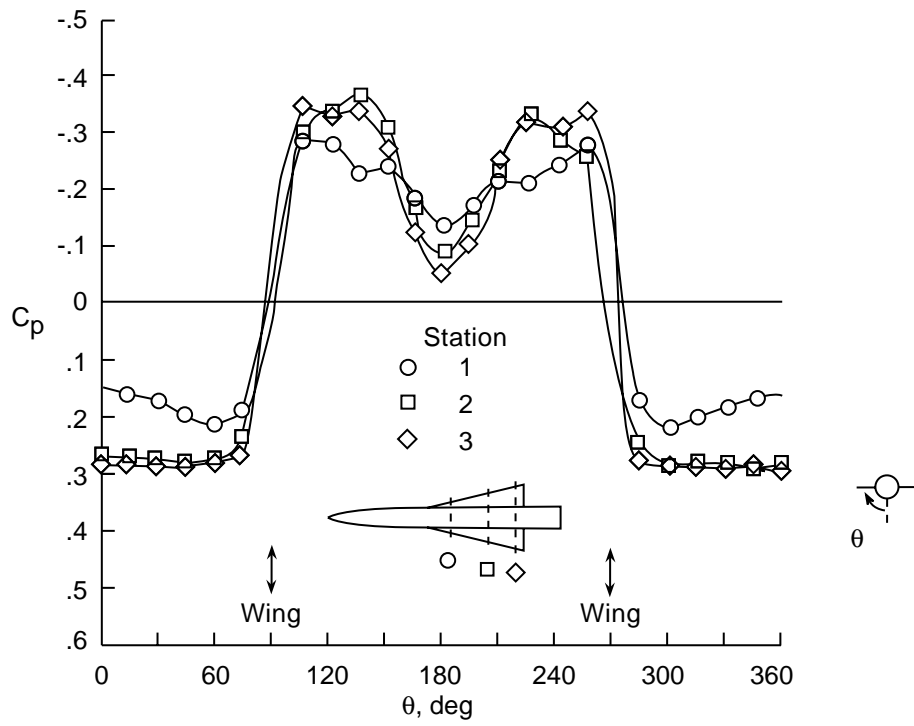


(a) Body.

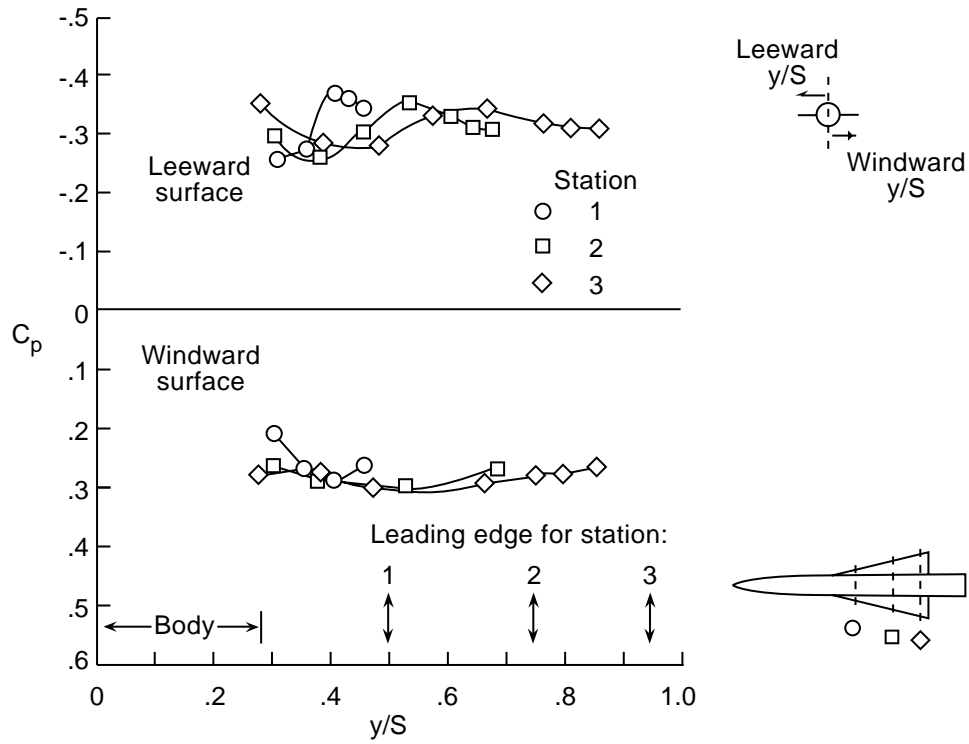


(b) Wing.

Figure 10. Effect of Mach number on station 3 of configuration 1 at $\alpha \approx 20^\circ$ and $\phi = 0^\circ$.

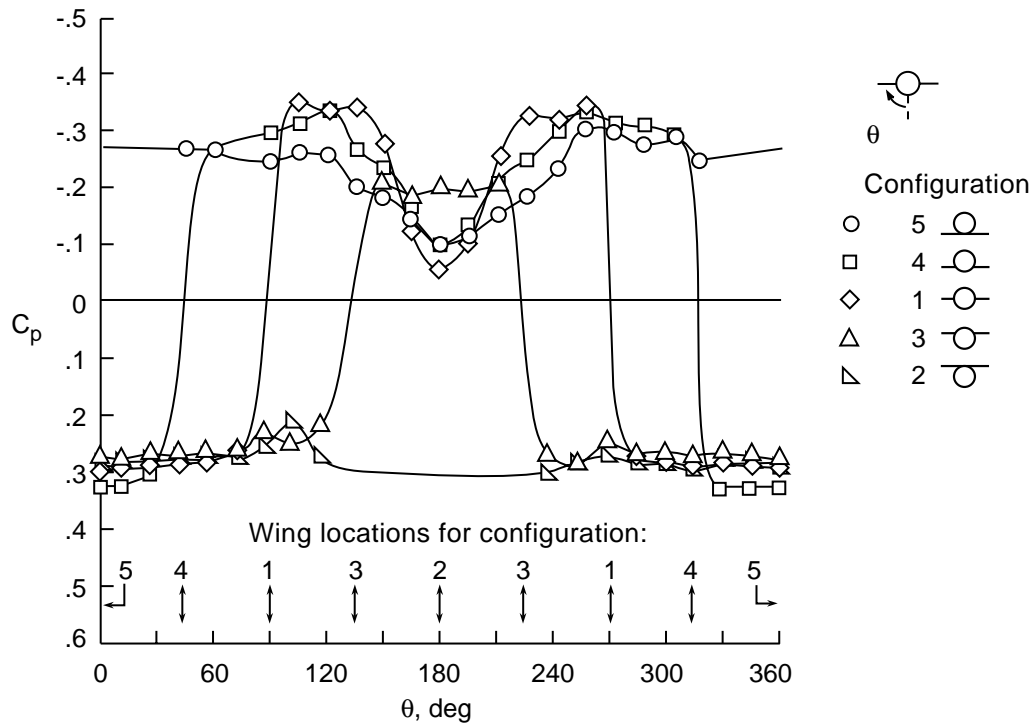


(a) Body.

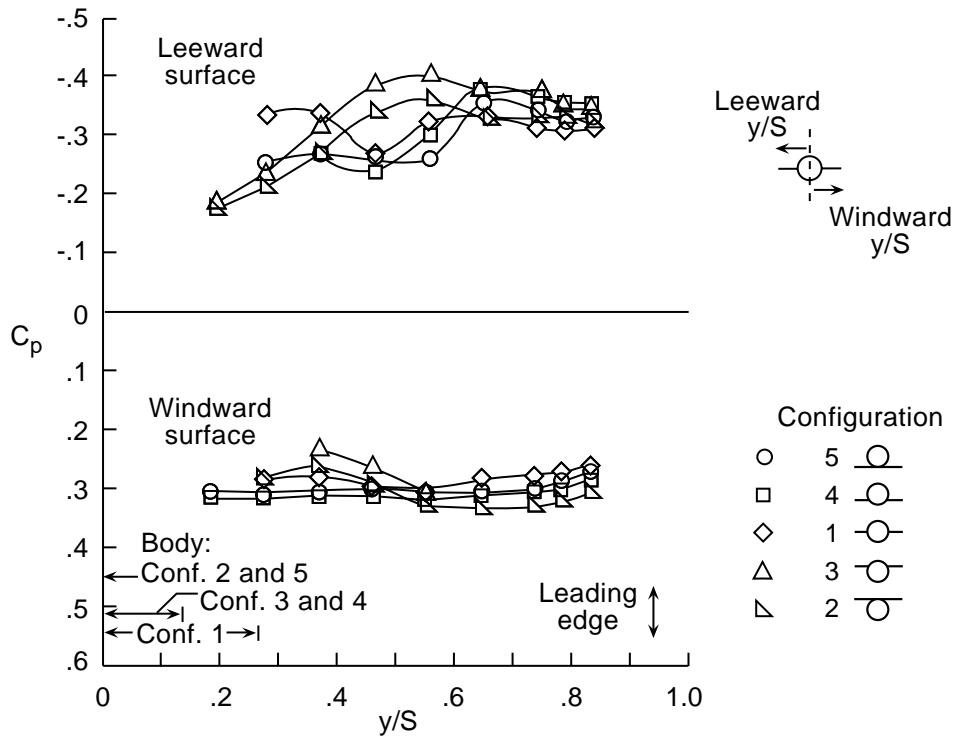


(b) Wing.

Figure 11. Effect of longitudinal station on configuration 1 at $M_\infty = 1.70$, $\alpha \approx 19.23^\circ$, and $\phi = 0^\circ$.

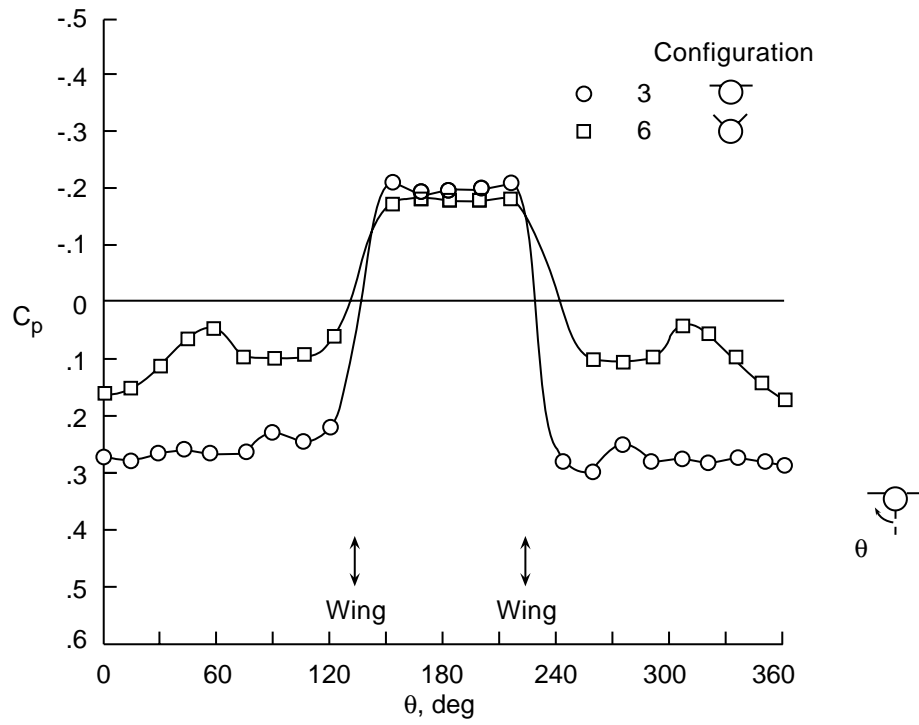


(a) Body.

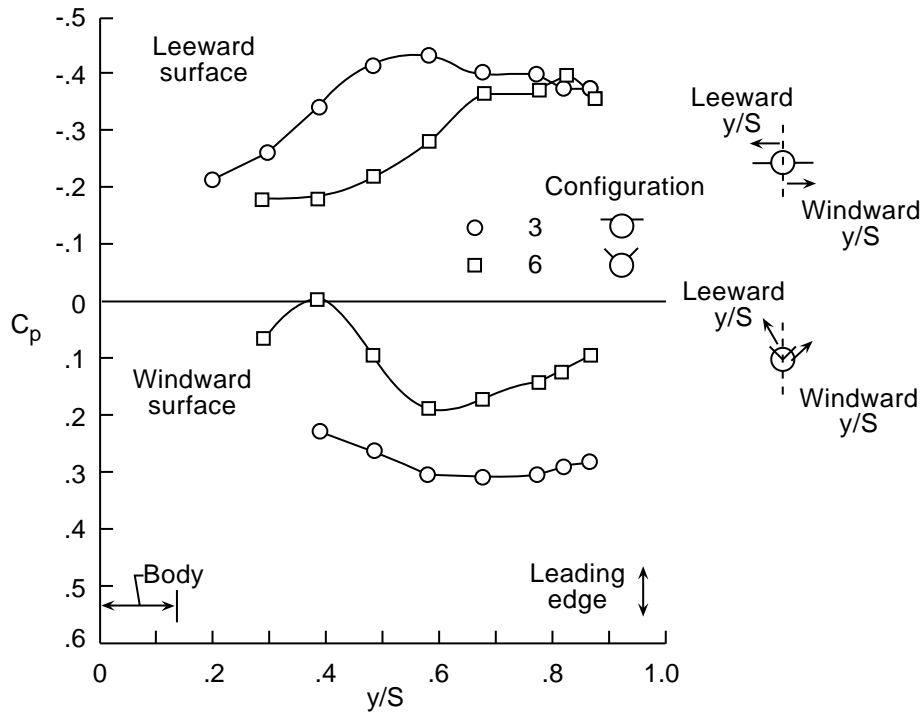


(b) Wing.

Figure 12. Effect of wing vertical location on station 3 at $M_\infty = 1.70$, $\alpha \approx 20^\circ$, and $\phi = 0^\circ$.

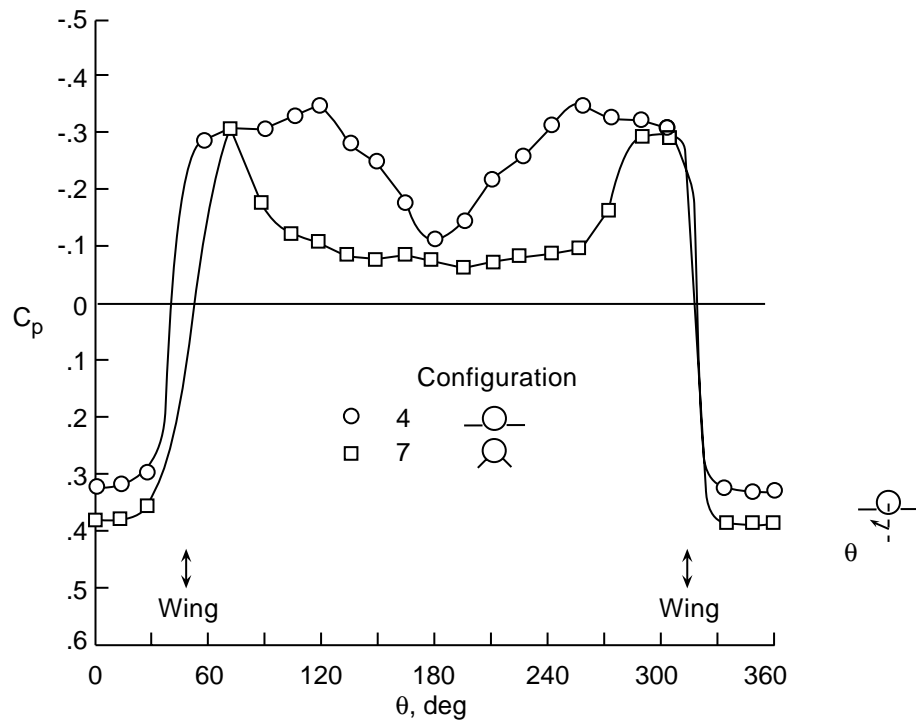


(a) Body.

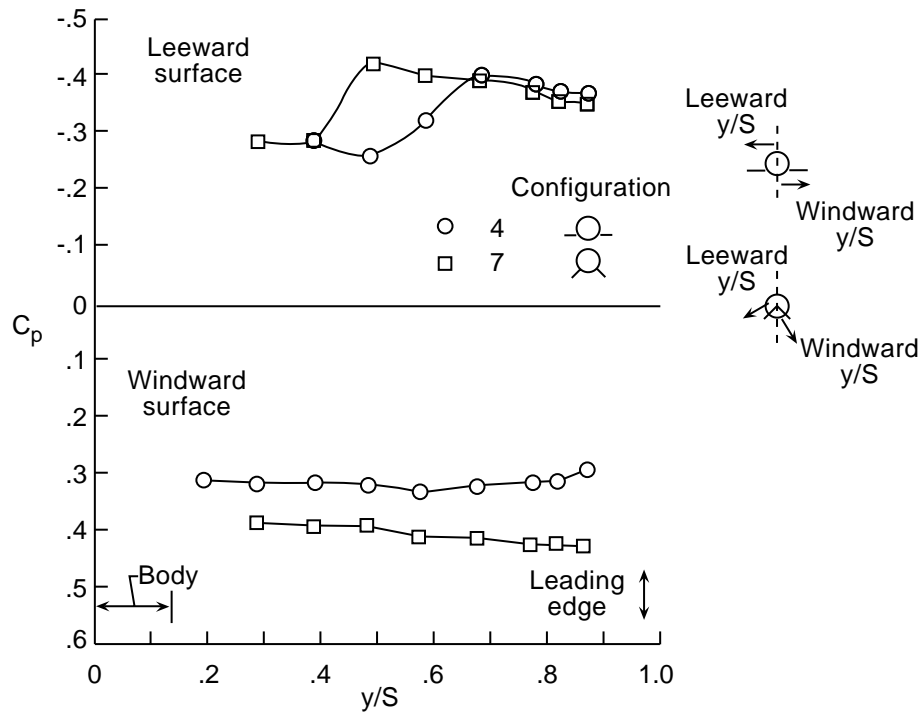


(b) Wing.

Figure 13. Wing angular orientation effect on station 3 for high-mounted wings at $M_\infty = 1.70$, $\alpha \approx 20^\circ$, and $\phi = 0^\circ$.

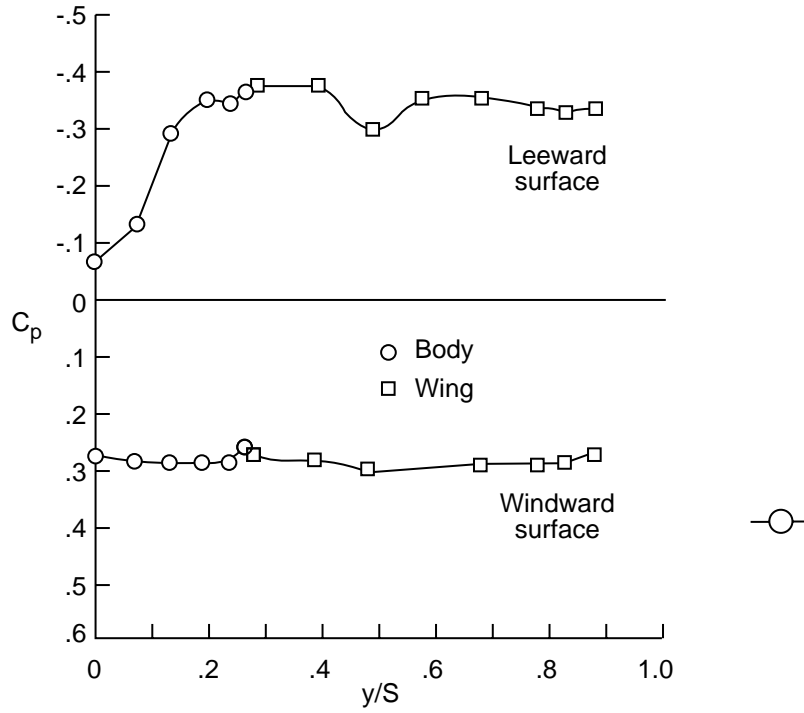


(a) Body.

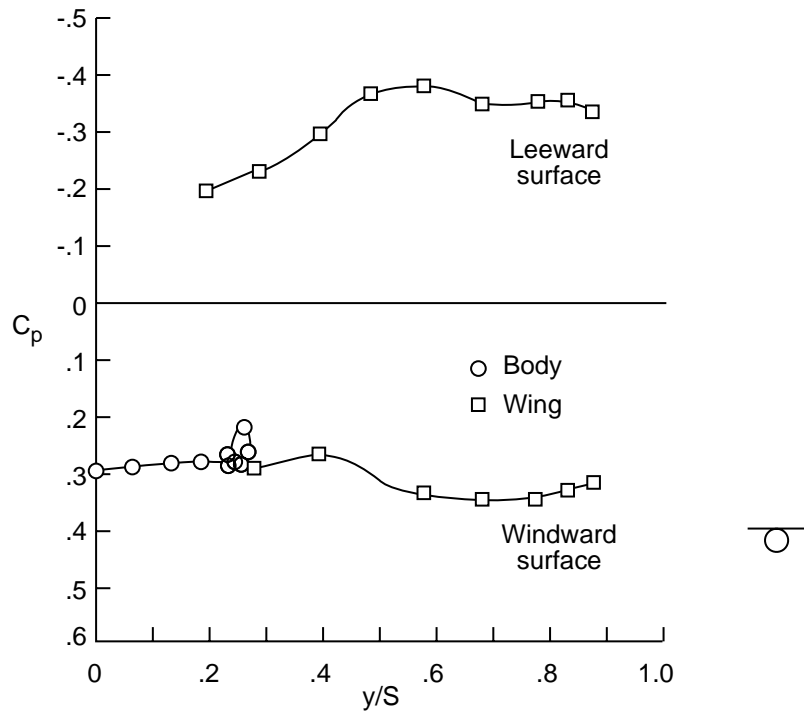


(b) Wing.

Figure 14. Wing angular orientation effect on station 3 for low-mounted wings at $M_\infty = 1.70$, $\alpha \approx 20^\circ$, and $\phi = 0^\circ$.

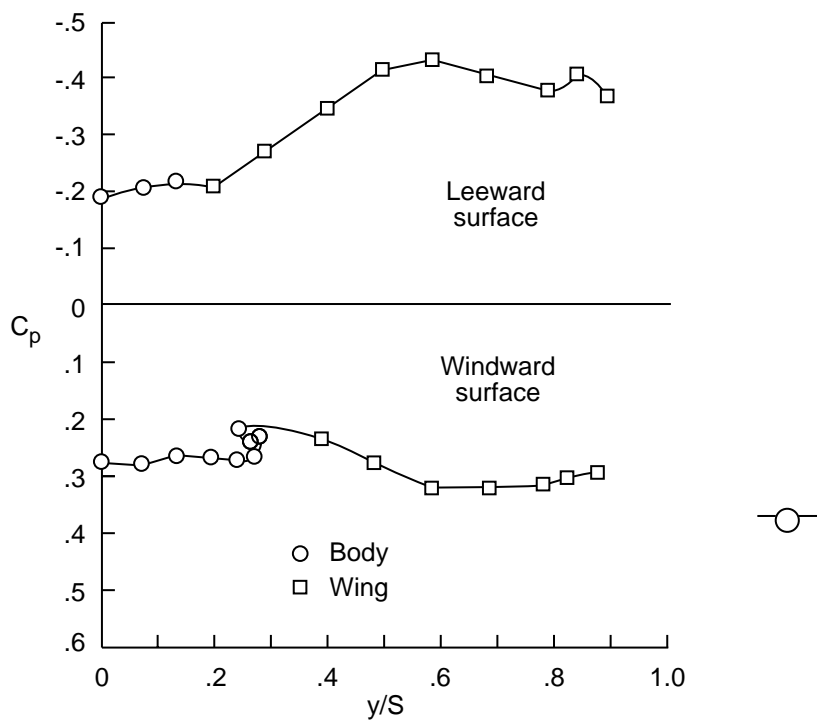


(a) Configuration 1 (baseline model).

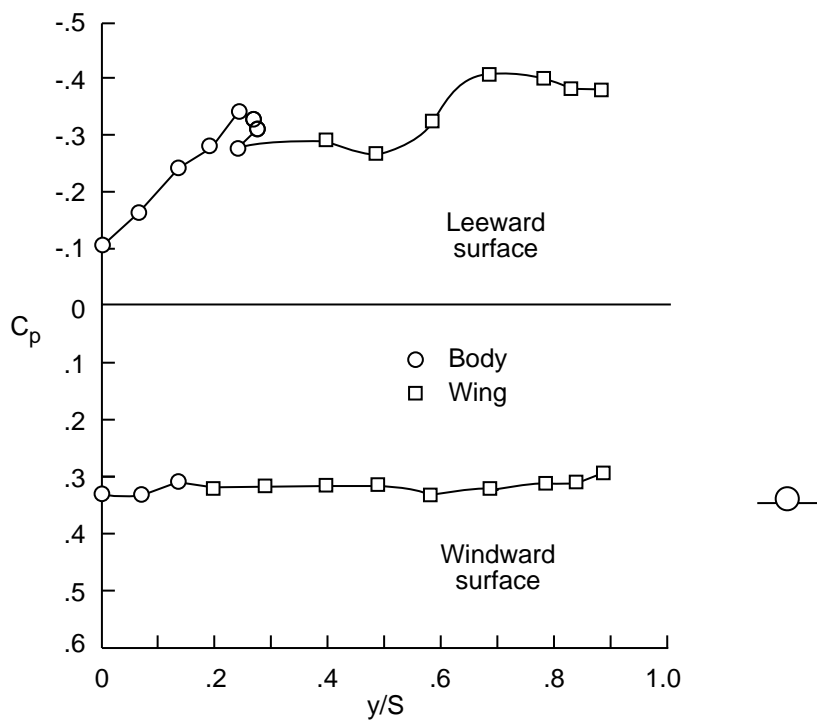


(b) Configuration 2.

Figure 15. Effect of wing-body juncture on station 3 at $M_\infty = 1.70$, $\alpha \approx 20^\circ$, and $\phi = 0^\circ$.

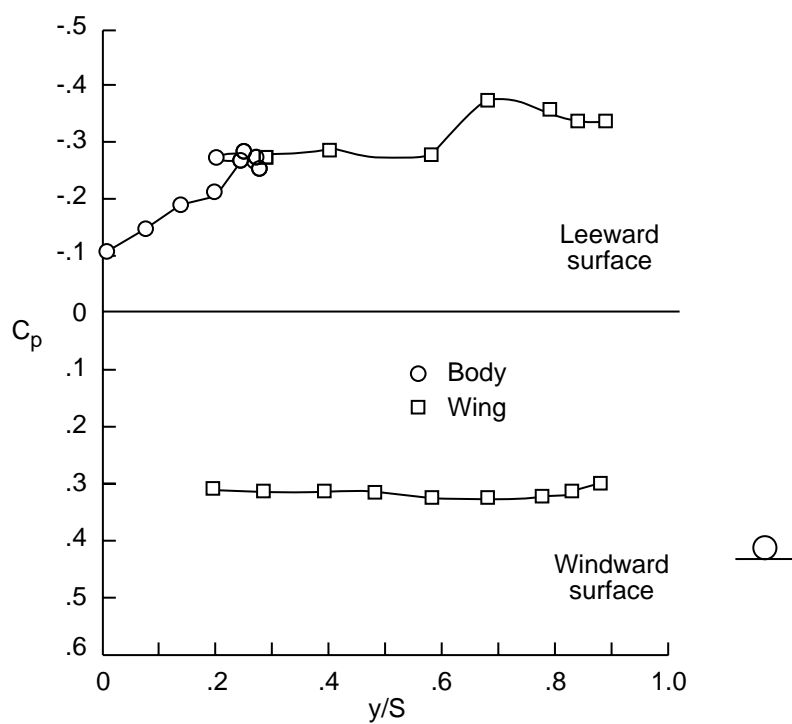


(c) Configuration 3.

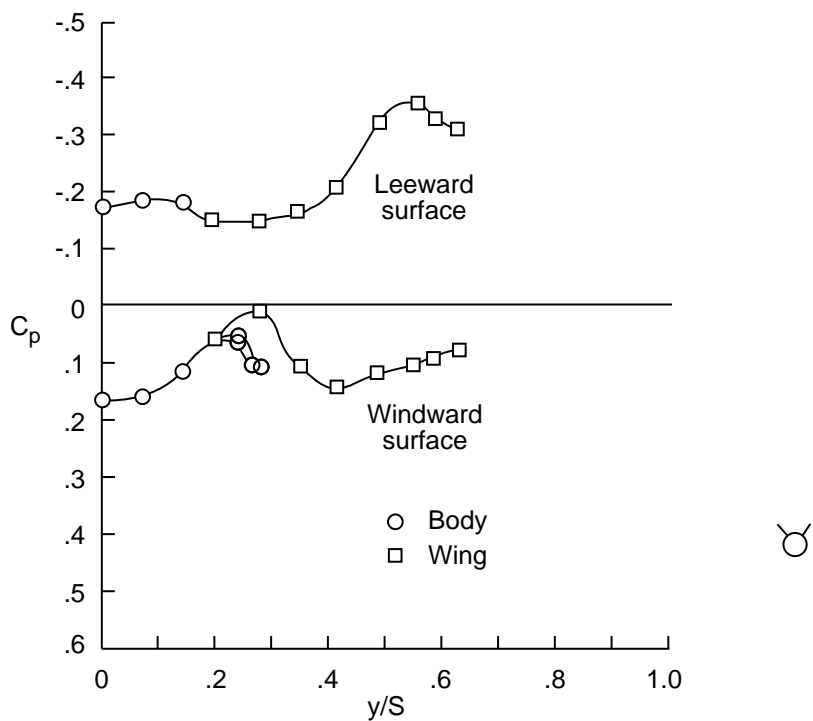


(d) Configuration 4.

Figure 15. Continued.

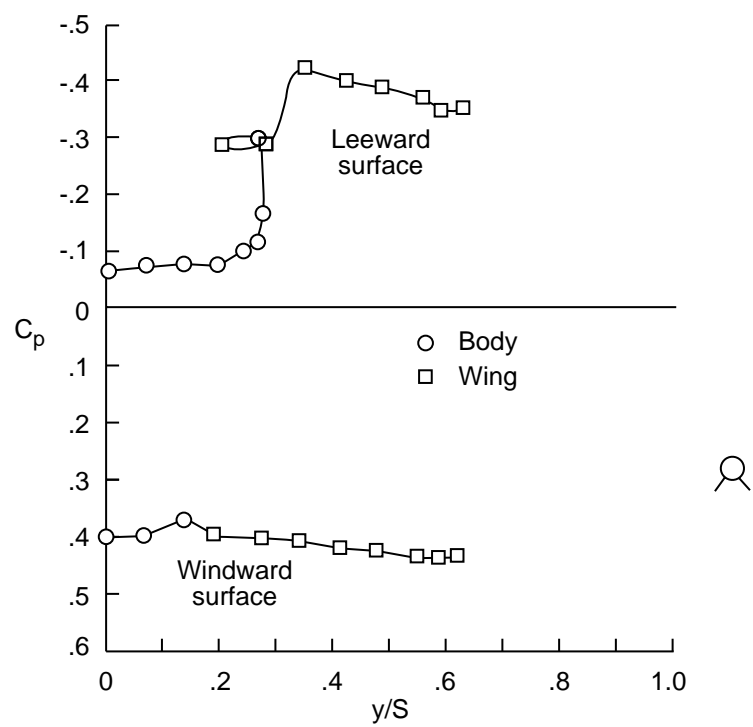


(e) Configuration 5.



(f) Configuration 6.

Figure 15. Continued.



(g) Configuration 7.

Figure 15. Concluded.

(a) Configuration 1 (baseline model). L-87-9272

(b) Configuration 2. L-87-8451

Figure 3. Photographs of configurations.

(c) Configuration 3. L-87-9273

(d) Configuration 4. L-87-9275

Figure 3. Continued.

(e) Configuration 5. L-87-8450

(f) Configuration 6. L-87-9274

Figure 3. Continued.

(g) Configuration 7. L-87-9276

(h) Configuration 8 (body alone). L-87-9271

Figure 3. Concluded.

Table 3. Configuration 1

(a) $M_\infty = 1.70; \phi = 0^\circ$; station 1

Table 3. Continued

(a) Continued; station 2

Table 3. Continued

(a) Concluded; station 3

Table 3. Continued

(b) $M_\infty = 2.16; \phi = 0^\circ$; station 1

Table 3. Continued

(b) Continued; station 2

Table 3. Continued

(b) Concluded; station 3

Table 3. Continued

(c) $M_\infty = 2.40; \phi = 0^\circ$; station 1

Table 3. Continued

(c) Continued; station 2

Table 3. Continued

(c) Concluded; station 3

Table 3. Continued

(d) $M_\infty = 2.86; \phi = 0^\circ$; station 1

Table 3. Continued

(d) Continued; station 2

Table 3. Continued

(d) Concluded; station 3

Table 3. Continued

(e) $M_\infty = 1.70; \phi = 30^\circ$; station 1

Table 3. Continued

(e) Continued; station 2

Table 3. Continued

(e) Concluded; station 3

Table 3. Continued

(f) $M_\infty = 2.16; \phi = 30^\circ$; station 1

Table 3. Continued

(f) Continued; station 2

Table 3. Continued

(f) Concluded; station 3

Table 3. Continued

(g) $M_\infty = 2.40; \phi = 30^\circ$; station 1

Table 3. Continued

(g) Continued; station 2

Table 3. Continued

(g) Concluded; station 3

Table 3. Continued

(h) $M_\infty = 2.86; \phi = 30^\circ$; station 1

Table 3. Continued

(h) Continued; station 2

Table 3. Continued

(h) Concluded; station 3

Table 3. Continued

(i) $M_\infty = 1.70; \phi = 60^\circ$; station 1

Table 3. Continued

(i) Continued; station 2

Table 3. Continued

(i) Concluded; station 3

Table 3. Continued

(j) $M_{\infty} = 2.16; \phi = 60^{\circ}$; station 1

Table 3. Continued

(j) Continued; station 2

Table 3. Continued

(j) Concluded; station 3

Table 3. Continued

(k) $M_{\infty} = 2.40; \phi = 60^{\circ}$; station 1

Table 3. Continued

(k) Continued; station 2

Table 3. Continued

(k) Concluded; station 3

Table 3. Continued

(l) $M_{\infty} = 2.86; \phi = 60^{\circ}$; station 1

Table 3. Continued

(l) Continued; station 2

Table 3. Continued

(l) Concluded; station 3

Table 3. Continued

(m) $M_{\infty} = 1.70; \phi = 90^{\circ}$; station 1

Table 3. Continued

(m) Continued; station 2

Table 3. Continued

(m) Concluded; station 3

Table 3. Continued

(n) $M_{\infty} = 2.16; \phi = 90^{\circ}$; station 1

Table 3. Continued

(n) Continued; station 2

Table 3. Continued

(n) Concluded; station 3

Table 3. Continued

(o) $M_\infty = 2.40; \phi = 90^\circ$; station 1

Table 3. Continued

(o) Continued; station 2

Table 3. Continued

(o) Concluded; station 3

Table 3. Continued

(p) $M_\infty = 2.86; \phi = 90^\circ$; station 1

Table 3. Continued

(p) Continued; station 2

Table 3. Continued

(p) Concluded; station 3

Table 3. Continued

(q) $M_\infty = 1.70; \phi = -30^\circ$; station 1

Table 3. Continued

(q) Continued; station 2

Table 3. Continued

(q) Concluded; station 3

Table 3. Continued

(r) $M_\infty = 2.16; \phi = -30^\circ$; station 1

Table 3. Continued

(r) Continued; station 2

Table 3. Continued

(r) Concluded; station 3

Table 3. Continued

(s) $M_\infty = 2.40; \phi = -30^\circ$; station 1

Table 3. Continued

(s) Continued; station 2

Table 3. Continued

(s) Concluded; station 3

Table 3. Continued

(t) $M_{\infty} = 2.86; \phi = -30^{\circ}$; station 1

Table 3. Continued

(t) Continued; station 2

Table 3. Continued

(t) Concluded; station 3

Table 3. Continued

(u) $M_{\infty} = 1.70; \phi = -60^{\circ}$; station 1

Table 3. Continued

(u) Continued; station 2

Table 3. Continued

(u) Concluded; station 3

Table 3. Continued

(v) $M_{\infty} = 2.16; \phi = -60^{\circ}$; station 1

Table 3. Continued

(v) Continued; station 2

Table 3. Continued

(v) Concluded; station 3

Table 3. Continued

(w) $M_{\infty} = 2.40; \phi = -60^{\circ}$; station 1

Table 3. Continued

(w) Continued; station 2

Table 3. Continued

(w) Concluded; station 3

Table 3. Continued

(x) $M_\infty = 2.86; \phi = -60^\circ$; station 1

Table 3. Continued

(x) Continued; station 2

Table 3. Continued

(x) Concluded; station 3

Table 3. Continued

(y) $M_\infty = 1.70; \phi = -90^\circ$; station 1

Table 3. Continued

(y) Continued; station 2

Table 3. Continued

(y) Concluded; station 3

Table 3. Continued

(z) $M_\infty = 2.16; \phi = -90^\circ$; station 1

Table 3. Continued

(z) Continued; station 2

Table 3. Continued

(z) Concluded; station 3

Table 3. Continued

(aa) $M_\infty = 2.40; \phi = -90^\circ$; station 1

Table 3. Continued

(aa) Continued; station 2

Table 3. Continued

(aa) Concluded; station 3

Table 3. Continued

(bb) $M_\infty = 2.86; \phi = -90^\circ$; station 1

Table 3. Continued

(bb) Continued; station 2

Table 3. Concluded

(bb) Concluded; station 3

Table 4. Configuration 2

(a) $M_\infty = 1.70$; station 1

Table 4. Continued

(a) Continued; station 2

Table 4. Continued

(a) Concluded; station 3

Table 4. Continued

(b) $M_\infty = 2.16$; station 1

Table 4. Continued

(b) Continued; station 2

Table 4. Continued

(b) Concluded; station 3

Table 4. Continued

(c) $M_\infty = 2.40$; station 1

Table 4. Continued

(c) Continued; station 2

Table 4. Continued

(c) Concluded; station 3

Table 4. Continued

(d) $M_\infty = 2.86$; station 1

Table 4. Continued

(d) Continued; station 2

Table 4. Concluded

(d) Concluded; station 3

Table 5. Configuration 3

(a) $M_\infty = 1.70$; station 1

Table 5. Continued

(a) Continued; station 2

Table 5. Continued

(a) Concluded; station 3

Table 5. Continued

(b) $M_\infty = 2.16$; station 1

Table 5. Continued

(b) Continued; station 2

Table 5. Continued

(b) Concluded; station 3

Table 5. Continued

(c) $M_\infty = 2.40$; station 1

Table 5. Continued

(c) Continued; station 2

Table 5. Continued

(c) Concluded; station 3

Table 5. Continued

(d) $M_\infty = 2.86$; station 1

Table 5. Continued

(d) Continued; station 2

Table 5. Concluded

(d) Concluded; station 3

Table 6. Configuration 4

(a) $M_\infty = 1.70$; station 1

Table 6. Continued

(a) Continued; station 2

Table 6. Continued

(a) Concluded; station 3

Table 6. Continued

(b) $M_\infty = 2.16$; station 1

Table 6. Continued

(b) Continued; station 2

Table 6. Continued

(b) Concluded; station 3

Table 6. Continued

(c) $M_\infty = 2.40$; station 1

Table 6. Continued

(c) Continued; station 2

Table 6. Continued

(c) Concluded; station 3

Table 6. Continued

(d) $M_\infty = 2.86$; station 1

Table 6. Continued

(d) Continued; station 2

Table 6. Concluded

(d) Concluded; station 3

Table 7. Configuration 5

(a) $M_\infty = 1.70$; station 1

Table 7. Continued

(a) Continued; station 2

Table 7. Continued

(a) Concluded; station 3

Table 7. Continued

(b) $M_\infty = 2.16$; station 1

Table 7. Continued

(b) Continued; station 2

Table 7. Continued

(b) Concluded; station 3

Table 7. Continued

(c) $M_\infty = 2.40$; station 1

Table 7. Continued

(c) Continued; station 2

Table 7. Continued

(c) Concluded; station 3

Table 7. Continued

(d) $M_\infty = 2.86$; station 1

Table 7. Continued

(d) Continued; station 2

Table 7. Concluded

(d) Concluded; station 3

Table 8. Configuration 6

(a) $M_\infty = 1.70$; station 1

Table 8. Continued

(a) Continued; station 2

Table 8. Continued

(a) Concluded; station 3

Table 8. Continued

(b) $M_\infty = 2.16$; station 1

Table 8. Continued

(b) Continued; station 2

Table 8. Continued

(b) Concluded; station 3

Table 8. Continued

(c) $M_\infty = 2.40$; station 1

Table 8. Continued

(c) Continued; station 2

Table 8. Continued

(c) Concluded; station 3

Table 8. Continued

(d) $M_\infty = 2.86$; station 1

Table 8. Continued

(d) Continued; station 2

Table 8. Concluded

(d) Concluded; station 3

Table 9. Configuration 7

(a) $M_\infty = 1.70$; station 1

Table 9. Continued

(a) Continued; station 2

Table 9. Continued

(a) Concluded; station 3

Table 9. Continued

(b) $M_\infty = 2.16$; station 1

Table 9. Continued

(b) Continued; station 2

Table 9. Continued

(b) Concluded; station 3

Table 9. Continued

(c) $M_\infty = 2.40$; station 1

Table 9. Continued

(c) Continued; station 2

Table 9. Continued

(c) Concluded; station 3

Table 9. Continued

(d) $M_\infty = 2.86$; station 1

Table 9. Continued

(d) Continued; station 2

Table 9. Concluded

(d) Concluded; station 3

Table 10. Configuration 8

(a) $M_\infty = 1.70$; station 1

Table 10. Continued

(a) Continued; station 2

Table 10. Continued

(a) Concluded; station 3

Table 10. Continued

(b) $M_\infty = 2.16$; station 1

Table 10. Continued

(b) Continued; station 2

Table 10. Continued

(b) Concluded; station 3

Table 10. Continued

(c) $M_\infty = 2.40$; station 1

Table 10. Continued

(c) Continued; station 2

Table 10. Continued

(c) Concluded; station 3

Table 10. Continued

(d) $M_\infty = 2.86$; station 1

Table 10. Continued

(d) Continued; station 2

Table 10. Concluded

(d) Concluded; station 3

REPORT DOCUMENTATION PAGE			Form Approved OMB No. 0704-0188	
Public reporting burden for this collection of information is estimated to average 1 hour per response, including the time for reviewing instructions, searching existing data sources, gathering and maintaining the data needed, and completing and reviewing the collection of information. Send comments regarding this burden estimate or any other aspect of this collection of information, including suggestions for reducing this burden, to Washington Headquarters Services, Directorate for Information Operations and Reports, 1215 Jefferson Davis Highway, Suite 1204, Arlington, VA 22202-4302, and to the Office of Management and Budget, Paperwork Reduction Project (0704-0188), Washington, DC 20503.				
1. AGENCY USE ONLY (Leave blank)		2. REPORT DATE April 1993		3. REPORT TYPE AND DATES COVERED Technical Memorandum
4. TITLE AND SUBTITLE Experimental Effects of Wing Location on Wing-Body Pressures at Supersonic Speeds			5. FUNDING NUMBERS WU 505-59-30-01	
6. AUTHOR(S) Jerry M. Allen and Carolyn B. Watson				
7. PERFORMING ORGANIZATION NAME(S) AND ADDRESS(ES) NASA Langley Research Center Hampton, VA 23681-0001			8. PERFORMING ORGANIZATION REPORT NUMBER L-17148	
9. SPONSORING/MONITORING AGENCY NAME(S) AND ADDRESS(ES) National Aeronautics and Space Administration Washington, DC 20546-0001			10. SPONSORING/MONITORING AGENCY REPORT NUMBER NASA TM-4434	
11. SUPPLEMENTARY NOTES				
12a. DISTRIBUTION/AVAILABILITY STATEMENT Unclassified-Unlimited Subject Category 02			12b. DISTRIBUTION CODE	
13. ABSTRACT (Maximum 200 words) An experimental study has been performed at supersonic speeds to measure wing and body spanwise pressure distributions on an axisymmetric-body delta wing model on which the wing vertical location on the body was systematically varied from low- to high-mounted positions. In addition, for two of these positions both horizontal and radial wing angular orientations relative to the body were tested, and roll angle effects were investigated for one of the positions. Seven different wing-body configurations and a body-alone configuration were studied. The test was conducted at Mach numbers from 1.70 to 2.86 at angles of attack from about -4° to 24° . Pressure orifices were located at three longitudinal stations on each wing-body model, and at each station the orifices were located completely around the body, along the lower surface of the right wing (looking upstream), and along the upper surface of the left wing. All pressure coefficient data are tabulated, and selected samples are shown graphically to illustrate the effects of the test variables. The effects of angle of attack, roll angle, Mach number, longitudinal station, wing vertical location, wing angular orientation, and wing-body juncture are analyzed. The vertical location of the wing on the body had a very strong effect on the body pressures. For a given angle of attack at a roll angle of 0° , the pressures were virtually constant in the spanwise direction across the windward surfaces of the wing-body combination. Pressure-relieving, channeling, and vortex effects were noted in the data.				
14. SUBJECT TERMS Wing-body aerodynamics; Experimental pressure distributions; Supersonic flow			15. NUMBER OF PAGES 196	
			16. PRICE CODE A09	
17. SECURITY CLASSIFICATION OF REPORT Unclassified	18. SECURITY CLASSIFICATION OF THIS PAGE Unclassified	19. SECURITY CLASSIFICATION OF ABSTRACT	20. LIMITATION OF ABSTRACT	